

Analytical model for electromagnetic cascades in rotating electric field

E. N. Nerush,* V. F. Bashmakov, and I. Yu. Kostyukov

Institute of Applied Physics, Russian Academy of Sciences, 603950 Nizhny Novgorod, Russia

Electromagnetic cascades attract a lot of attention as an important QED effect that will reveal itself in various electromagnetic field configurations at ultrahigh intensities. We study cascade dynamics in rotating electric field analytically and numerically. The kinetic equations for the electron-positron plasma and gamma-quanta are formulated. The scaling laws are derived and analyzed. For the cascades arising far above the threshold the dependence of the cascade parameters on the field frequency is derived. The spectra of high-energy cascade particles are calculated. The analytical results are verified by numerical simulations.

PACS numbers: 12.20.-m, 42.50.Ct, 52.27.Ep, 52.25.Dg

Keywords: electromagnetic cascades, strong laser field, kinetic equations, Monte Carlo simulations

I. INTRODUCTION

Quantum electrodynamics (QED) effects in a strong electromagnetic field attract a lot of attention [1, 2]. In the last decade a new surge of interest in QED effects in superstrong electromagnetic field arises thanks to substantial progress in laser technologies [3–5]. Theoreticians are considering such effects as vacuum polarization in laser field [6], electron-positron (e^+e^-) pair production from vacuum in the field of colliding laser pulses [7] and in combined Coulomb and strong laser field [8] etc.

Up to now the electromagnetic fields are not so intense in laboratory to observe strong-field QED effects directly. However, the interaction of ultra-high energy electron beams with electromagnetic fields can be used to study the effects as in the frame of the relativistic electron the electromagnetic field can be very strong. The spectra of the scattered electrons and photons arising from the nonlinear Compton scattering of intense laser pulse by 46.6 GeV electron beam have been measured experimentally [9, 10]. The e^+e^- pair production has been also observed. The strong-field QED effects like channeling radiation and e^+e^- pair production at the interaction of relativistic electron beam with crystalline fields has been also studied experimentally and theoretically [11, 12]. A number of theoretical and numerical models for QED effects accompanying an interaction of relativistic electrons with strong electromagnetic fields has been developed. The evolution of the distribution functions of electrons, positrons and hard photons in QED-strong pulsed laser fields interacting with electron beams were found numerically [13]. In Ref. [14] multiphoton trident pair production in strong laser field was studied in a manifestly nonperturbative domain in the periodic plane wave approximation. In addition, the energy spectrum of positrons produced in collision of strong laser pulse with high-energy electron beam was calculated. The trident pair production amplitude in a strong laser background

was also calculated in Ref. [15]. As opposed to [14], the finite pulse durations were allowed, while the laser fields were still treating nonperturbatively in strong-field QED. The individual contributions of the one-step and two-step processes were explicitly identified.

Another effect that can be very important at high intensities is the generation of electromagnetic cascades [16, 17]. The cascades develop as follows. A slow electron can be accelerated in superstrong laser fields up to very high energy. Then it can produce a high-energy photon γ by Compton scattering with n laser photons involved in the process:

$$e + n\omega \rightarrow e' + \gamma. \quad (1)$$

The resulting photon creates a pair in a photon-multiphoton collision:

$$\gamma + n\omega \rightarrow e^+e^-. \quad (2)$$

This reaction can be considered as the strong-field generalization of the Breit–Wheeler process [2, 18]. The produced electron and positron as well as the initial (seed) electron are accelerated by the field and become capable to produce new high-energy photons by the process (1). Hence, the number of the particles grows rapidly due to the deposition of the laser energy into the particle acceleration. As a result, the relativistic electron-positron-gamma plasma is produced. Besides pair creation by consecutive processes (1) and (2), the particle multiplication can occur by the process of Bethe–Heitler type (or trident process) [2, 19]: $e + n\omega \rightarrow e'e^+e^-$. However, the threshold intensity for cascade development is about $I \sim 10^{25}$ W/cm², and for modern laser system the characteristic wavelength is about $\lambda_l \sim 1$ μ m. At such parameters the overall probability of processes (1) and (2) are much higher than the probability of the Bethe–Heitler process.

The seed e^+e^- pair can be created as a result of the instability of QED vacuum in strong electromagnetic field [7, 20–22]. The probability of the vacuum pair creation increases in the field of two colliding laser pulses [23, 24] or in the focused laser pulse [25]. However, the threshold intensity for the pair creation by colliding and focused

*Electronic address: nerush@appl.sci-nnov.ru

laser pulses with $\lambda_l \simeq 1 \mu\text{m}$ is very high and can be up to $2.3 \times 10^{26} \text{ W/cm}^2$ for the pulse duration 10 fs and circular polarization [26]. The use of high-energy photons as a seed for the cascade is more preferable than that of free electrons and positrons because the ponderomotive force of the laser pulses pushes the charged particles out from the high-intensity region. The seed particles can be also produced by atom ionization [27] or pair production in the superposition of laser field and the Coulomb field of heavy nuclei [8]. When the number of the created cascade particles becomes large the plasma effects are important and the significant amount of the laser energy can be absorbed due to production and heating of the electron-positron pair plasma. This can limit the attainable intensity of high-power lasers [17, 28].

The dimensionless parameters characterizing QED effects can be introduced [29, 30]:

$$a_0 = \frac{e\sqrt{-A_\mu A^\mu}}{mc}, \quad (3)$$

$$\chi_{e,\gamma} = \frac{e\hbar}{m^3 c^4} |F_{\mu\nu} p^\nu| \simeq \frac{(\mathbf{E} + [\mathbf{v}/c, \mathbf{B}])_\perp}{E_{cr}} \gamma, \quad (4)$$

where A_μ is the 4-vector of the field potential, \mathbf{E} and \mathbf{B} are the electric and magnetic field strength, respectively, $F_{\mu\nu}$ is the field-strength tensor, p^ν is the particle four-momentum, γ is the particle Lorentz factor ($\gamma = \hbar\omega/mc^2$ for the photon), \mathbf{v} is the particle velocity, $E_{cr} = m^2 c^3 / e\hbar$ is the QED critical field strength, $e > 0$ is the value of electron charge, m is the electron mass, c is the speed of light, \hbar is the Planck constant, ω is the photon frequency, ω_l is the laser frequency, symbol \perp denotes the component which is perpendicular to the particle velocity. The first parameter a_0 characterizes the laser field strength. If the laser field is weak $a_0 \ll 1$ then mostly $n = 1$ in Eqs. (1) and (2). In the opposite limit $a_0 \gg 1$ the electron absorbs a large number of photons and the radiation spectrum becomes synchrotron-like [30]. The second parameter χ_e characterizes the regime of the photon emission. In the limit $\chi_e \ll 1$ the radiation can be described classically (except the case when the number of the emitted photons is small, see Ref. [31]) while in the opposite limit the recoil imposed on the electron by the emitted photon is substantial and the quantum approach should be used. Similarly, pair production is significant in the limit $\chi_\gamma \gg 1$ while it is exponentially suppressed in the classical limit $\chi_\gamma \ll 1$.

At high intensity the so-called radiation formation length [29] becomes much smaller than the laser wavelength and the characteristic path passed by the electron between two consecutive photon emissions. This regime is often referred as quasistatic or tunneling and can be treated in the framework of quasiclassical approach [11, 29]. The Compton scattering is treated just as the transition of the electron from one level to another in external constant and homogeneous electromagnetic field that is accompanied by photon emission. The pair production is considered similarly. In addition, the quasiclassical approach implies that the particles moves along

the classical trajectories between the instances of photon emission or pair production that strongly simplifies calculations.

Quantum dynamics of the particles and their interaction are complex phenomena and a number of numerical models is proposed. There are numerical models based on the first principles like solving Dirac's equation and calculating the cross-sections of QED processes [32]. To simulate collective dynamics of the particles the numerical solution of the kinetic equations can be used [13]. Another probably more numerically efficient approach is provided by Monte Carlo methods. A number of sophisticated models like well-known Geant4 toolkit for the simulation of the passage of particles through matter [33] are based on Monte Carlo methods. Monte Carlo calculations are also used to analyze the cascade development in the strong electromagnetic fields [34, 35]. Recently particle-in-cell methods have been also used to simulate the effect of the self-generated electromagnetic fields of the produced e^+e^- pairs on the cascade development [28, 36].

In this paper we examine and solve analytically the kinetic equations for the particle distribution functions in the electromagnetic cascade in the homogeneous rotating electric field. This is one of the most simple field configuration where electromagnetic cascades arise. Besides, the rotating electric field can be found in the B -node of the circularly polarized standing wave formed by two co-propagating circularly polarized laser pulses. The plane $B = 0$ is the most favorable for the cascade development. However, for the simplicity we consider homogeneous electric field. In order to analyze the particle distribution we use the following assumptions: (i) we use the quasiclassical synchrotron formulae for the probabilities of photon emission and pair production, and neglect the angles $\lesssim 1/\gamma$; (ii) the probability rates are averaged over the polarization of the particles; (iii) the self-generated electromagnetic fields of the particles produced in the cascade are neglected. The last assumption is valid at the initial stages of the cascade development when the density of the self-generated electron-positron pair plasma is not high [28]. Under the assumption that the number of the cascade particles doubles many times on the period of the field rotation the analytical solutions for the distribution functions are obtained for the region in the phase space $\gamma \gg \langle \gamma \rangle$ and $\chi \gg 1$, where $\langle \gamma \rangle$ is the average relativistic factor of the cascade particles. The obtained solution is used to calculate the energy spectra of the electrons, the positrons and the photons. The analytical results are compared with the results of the numerical simulations performed using the particle-in-cell Monte Carlo technique described in Ref. [28].

The paper is organized as follows. In Sec. II we consider the electron, positron and photon motion in the rotating electric field. In Sec. III the cascade kinetic equations for the particle distribution functions are discussed. The cascade scalings are derived and discussed in Sec. IV and Sec. V. The distribution functions of the cascade

particles are derived in Sec. VI. In Sec. VII the obtained results are verified by the numerical simulations and the asymptotic formulae for the particle spectra are given in Sec. VIII. Finally, in Sec. IX summary and discussion are given.

II. PARTICLE MOTION IN THE ABSENCE OF PHOTON EMISSION AND PAIR PRODUCTION

First we study particle motion in the rotating electric field in the framework of the classical approach, neglecting photon emission and e^+e^- pair production. The field components are the following:

$$E_x = E_0 \cos(t + \phi_0), \quad (5)$$

$$E_y = E_0 \sin(t + \phi_0), \quad (6)$$

that leads to the following equations of motion

$$\frac{dp_x}{dt} = -\cos(t + \phi_0), \quad (7)$$

$$\frac{dp_y}{dt} = -\sin(t + \phi_0), \quad (8)$$

where x, y are the Cartesian coordinates normalized to c/ω_l in the plane of the rotation of the vector \mathbf{E} , t normalized to $1/\omega_l$, \mathbf{p} is the electron momentum normalized to $mca_0 = eE_0/\omega_l$, and ϕ_0 is initial phase. We are interested only in particle dynamics in the momentum space so far as the electric field is homogeneous. We introduce ψ universally for all species of the particles as the angle between $-\mathbf{E}$ and \mathbf{p} . Small and positive values of ψ mean that particle lags behind the vector $-\mathbf{E}$ in the rotation. Then we have: $p_x = -p \cos(t + \phi_0 - \psi)$, $p_y = -p \sin(t + \phi_0 - \psi)$, and Eqs. (7) and (8) can be rewritten as follows

$$\frac{d\psi}{dt} = 1 - \frac{\sin \psi}{p}, \quad (9)$$

$$\frac{dp}{dt} = \cos \psi. \quad (10)$$

These equations can be reduced to the single equation in the plane $p - \psi$:

$$\frac{d(\sin \psi)}{dp} = 1 - \frac{\sin \psi}{p}, \quad (11)$$

The solution of the equation is the following:

$$\sin \psi = \frac{p}{2} + \frac{p_0}{p} \left(\sin \psi_0 - \frac{p_0}{2} \right), \quad (12)$$

where p_0 and ψ_0 are the initial values of the electron momentum and the angle, respectively. The electron trajectories (12) are shown in Fig. 1 (a). The positron trajectories (Fig. 1 (b)) can be obtained from Eq. (12) by the

substitution $\psi \rightarrow \psi - \pi$. What this means is the positrons are accelerated in the opposite direction to the electron acceleration direction. The photon momentum does not change during the propagation, and the angle ψ for a photon grows linearly in the course of time $\psi = \psi_0 + t$. Corresponding trajectories are shown in Fig. 1 (c).

The restoration of the particle energy in the cascade can be illustrated using Fig. 1. Let us consider initially immobile electron. At first, from the point $\psi = 0, \gamma = 0$ it is being accelerated along the bold line in Fig. 1 (a) (separatrix): $p \approx t$ and $\sin \psi = p/2$. Then it emits a photon and shifts left: its angle ψ remains the same and its gamma-factor decreases due to the photon emission. Next according to the phase flow the electron comes again to the separatrix. This also explains why the electrons are concentrated near the separatrix.

As we will see below, the electron distribution function drops along this line due to the following reasons. First, some of the electrons emit photons and leave the separatrix. Second, the acceleration of the electrons that have higher energy starts earlier in the average than the acceleration of the electrons with lower energies. The number of particles is increasing exponentially with time in the cascade, hence, the number of particles that gain higher energy is lower.

III. BASIC EQUATIONS

The cascade kinetic equations have been derived a long time ago to study development of showers initiated by cosmic rays in the Earth's atmosphere [38, 39]. The shower (avalanche) develops due to the bremsstrahlung and pair production at the particle interaction with nuclei. The solution of the equations has been obtained in Ref. [38]. Later the solution method has been extended to include multiphoton processes [40] and to study the electromagnetic showers in strong magnetic field [41]. The kinetic approach have been used in numerical simulations to analyze the interaction of the intense laser pulse with the electron beam [13]. The kinetic equations have been also formulated for the problem of the cascade development in the laser field and have been used to derive radiation reaction force [42] in classical limit in Ref. [37]. However, up to now the kinetic cascade equations have been analytically solved only in one-dimensional cases. On the contrary, we consider theoretically and numerically the two-dimensional cascade. Moreover, we will take into account that the overall energy of the cascade particles is growing and can be much more than the seed particle energy.

The cascade kinetic equations in arbitrary field can be written as follows:

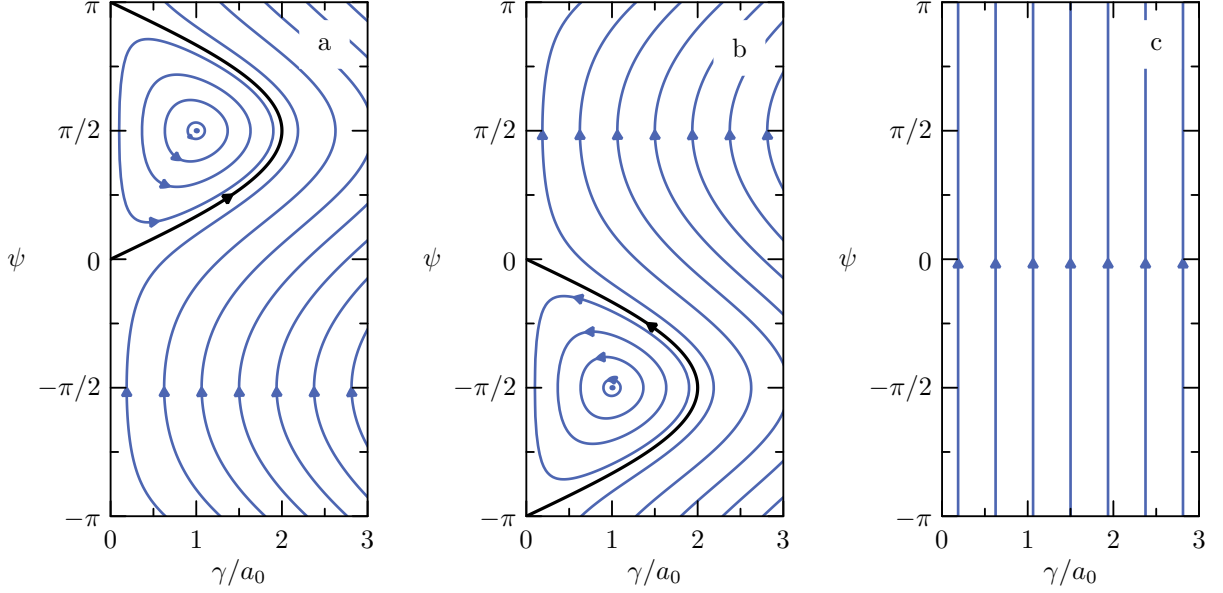


Figure 1: The trajectories in $p - \psi$ space for (a) electrons, (b) positrons and (c) photons moving in the rotating electric field. Photon emission and pair production are not taken into account. The bold lines correspond to the trajectories which separate bounded and open trajectories.

$$\begin{aligned} \partial_t f_e(\mathbf{r}, \mathbf{p}) + \frac{\mathbf{p}}{p} \nabla f_e(\mathbf{r}, \mathbf{p}) + \nabla_{\mathbf{p}} \{f_e(\mathbf{r}, \mathbf{p}) \times \mathbf{F}_e(\mathbf{r}, \mathbf{p})\} &= \int_{\mathbf{p}' \parallel \mathbf{p}} \frac{p'^{D-1}}{p^{D-1}} f_\gamma(\mathbf{r}, \mathbf{p}') \tilde{w}(\mathbf{p}' \rightarrow \mathbf{p}) dp' \\ &+ \int_{\mathbf{p}' \parallel \mathbf{p}} \frac{p'^{D-1}}{p^{D-1}} f_e(\mathbf{r}, \mathbf{p}') w(\mathbf{p}' \rightarrow \mathbf{p}) dp' - \int_{\mathbf{p}' \parallel \mathbf{p}} f_e(\mathbf{r}, \mathbf{p}) w(\mathbf{p} \rightarrow \mathbf{p}') dp', \quad (13) \end{aligned}$$

$$\begin{aligned} \partial_t f_p(\mathbf{r}, \mathbf{p}) + \frac{\mathbf{p}}{p} \nabla f_p(\mathbf{r}, \mathbf{p}) + \nabla_{\mathbf{p}} \{f_p(\mathbf{r}, \mathbf{p}) \times \mathbf{F}_p(\mathbf{r}, \mathbf{p})\} &= \int_{\mathbf{p}' \parallel \mathbf{p}} \frac{p'^{D-1}}{p^{D-1}} f_\gamma(\mathbf{r}, \mathbf{p}') \tilde{w}(\mathbf{p}' \rightarrow \mathbf{p}' - \mathbf{p}) dp' \\ &+ \int_{\mathbf{p}' \parallel \mathbf{p}} \frac{p'^{D-1}}{p^{D-1}} f_p(\mathbf{r}, \mathbf{p}') w(\mathbf{p}' \rightarrow \mathbf{p}) dp' - \int_{\mathbf{p}' \parallel \mathbf{p}} f_p(\mathbf{r}, \mathbf{p}) w(\mathbf{p} \rightarrow \mathbf{p}') dp', \quad (14) \end{aligned}$$

$$\begin{aligned} \partial_t f_\gamma(\mathbf{r}, \mathbf{p}) + \frac{\mathbf{p}}{p} \nabla f_\gamma(\mathbf{r}, \mathbf{p}) &= - \int_{\mathbf{p}' \parallel \mathbf{p}} f_\gamma(\mathbf{r}, \mathbf{p}') \tilde{w}(\mathbf{p} \rightarrow \mathbf{p}') dp' \\ &+ \int_{\mathbf{p}' \parallel \mathbf{p}} \frac{p'^{D-1}}{p^{D-1}} f_e(\mathbf{r}, \mathbf{p}') w(\mathbf{p}' \rightarrow \mathbf{p}' - \mathbf{p}) dp' + \int_{\mathbf{p}' \parallel \mathbf{p}} \frac{p'^{D-1}}{p^{D-1}} f_p(\mathbf{r}, \mathbf{p}') w(\mathbf{p}' \rightarrow \mathbf{p}' - \mathbf{p}) dp', \quad (15) \end{aligned}$$

where \mathbf{r} is the particle coordinate normalized to c/ω_l , \mathbf{F} is the Lorentz force normalized to $a_0 m c \omega_l$, D is the space dimension, f_e , f_p and f_γ are the distribution functions of the electrons, the positrons and the photons, respectively, which are normalized such that

$$\int f_{e,p,\gamma}(\mathbf{r}, \mathbf{p}) d^D \mathbf{r} d^D \mathbf{p} = N_{e,p,\gamma}, \quad (16)$$

where N_e , N_p , N_γ is the number of the electrons, the

positrons and the photons, respectively. $w(\mathbf{p}' \rightarrow \mathbf{p}) dp$ is the probability in time unit for the electron with momentum \mathbf{p}' to emit a photon and to switch to the state with the value of momentum in the interval $(p, p + dp)$ and the direction of the momentum parallel to \mathbf{p}' , $\tilde{w}(\mathbf{p}' \rightarrow \mathbf{p}) dp$ is the probability in time unit for the photon with momentum \mathbf{p}' to decay with creation of the electron with momentum in the interval $(p, p + dp)$ directed parallel to \mathbf{p}' and the positron with momentum $\mathbf{p}' - \mathbf{p}$. Here we as-

sume that the photon emission and the pair production occur in synchrotron regime, and we neglect the angles less or about than $1/\gamma$. Dependences of $f_{e,p,\gamma}$, \mathbf{F} on t and w , \tilde{w} on \mathbf{F} are not written for the simplicity.

The RHS of Eqs. (13)-(15) describes photon emission and pair production. Namely, the first term in the RHS of Eq. (13) characterizes creation of the electrons with momentum \mathbf{p} by decay of the photons with momenta $p' > p$, the second and the third terms respectively describe the increase and decrease of the number of the electrons with momentum \mathbf{p} due to photon emission. The first term in the RHS of Eq. (15) characterizes photon decay, and the last two terms describe emission of new photons by the electrons and the positrons.

The kinetic equations in the rotating electric field (5), (6) in the plane geometry ($D = 2$) can be written as follows [37]:

$$\begin{aligned} & \partial_t f_{e,p}(\mathbf{p}) \mp \cos(t + \phi_0) \frac{\partial f_{e,p}(\mathbf{p})}{\partial p_x} \\ & \mp \sin(t + \phi_0) \frac{\partial f_{e,p}(\mathbf{p})}{\partial p_y} = \int_{\mathbf{p}' \parallel \mathbf{p}} \frac{p'}{p} f_\gamma(\mathbf{p}') \tilde{w}(\mathbf{p}' \rightarrow \mathbf{p}) dp' + \\ & \int_{\mathbf{p}' \parallel \mathbf{p}} \frac{p'}{p} f_{e,p}(\mathbf{p}') w(\mathbf{p}' \rightarrow \mathbf{p}) dp' - W(\mathbf{p}) f_{e,p}(\mathbf{p}), \end{aligned} \quad (17)$$

$$\begin{aligned} \partial_t f_\gamma(\mathbf{p}) &= -\tilde{W}(\mathbf{p}) f_\gamma(\mathbf{p}) \\ &+ \int_{\mathbf{p}' \parallel \mathbf{p}} \frac{p'}{p} f_e(\mathbf{p}') w(\mathbf{p}' \rightarrow \mathbf{p}' - \mathbf{p}) dp' \\ &+ \int_{\mathbf{p}' \parallel \mathbf{p}} \frac{p'}{p} f_p(\mathbf{p}') w(\mathbf{p}' \rightarrow \mathbf{p}' - \mathbf{p}) dp', \end{aligned} \quad (18)$$

where the relation $\tilde{w}(\mathbf{p}' \rightarrow \mathbf{p}' - \mathbf{p}) = \tilde{w}(\mathbf{p}' \rightarrow \mathbf{p})$ is taken into account, "−" in "∓" corresponds to the equation for the electron distribution function and "+" corresponds to the equation for the positron distribution function,

$$f_{e,p,\gamma}(\mathbf{p}) = \int f_{e,p,\gamma}(\mathbf{r}, \mathbf{p}) d^2 \mathbf{r}, \quad (19)$$

$$W(\mathbf{p}) = \int w(\mathbf{p} \rightarrow \mathbf{p}') dp', \quad (20)$$

$$\tilde{W}(\mathbf{p}) = \int \tilde{w}(\mathbf{p} \rightarrow \mathbf{p}') dp'. \quad (21)$$

In order to eliminate the dependence of the force and the probabilities on time in Eqs. (17) and (18), we make the change of variables $p_x, p_y \rightarrow p, \psi$ as follows. Introducing particle distribution functions in new variables

$$\begin{aligned} g_{e,p,\gamma}(t, p, \psi) &= p f_{e,p,\gamma}(t, p_x, p_y) = \\ p f_{e,p,\gamma}(t, -p \cos(t + \phi_0 - \psi), -p \sin(t + \phi_0 - \psi)), \end{aligned} \quad (22)$$

we obtain:

$$\frac{\partial g_{e,p,\gamma}}{\partial t} = p \frac{\partial f_{e,p,\gamma}}{\partial t} - \frac{\partial g_{e,p,\gamma}}{\partial \psi}, \quad (23)$$

$$\begin{aligned} \cos(t + \phi_0) \frac{\partial f_{e,p}}{\partial p_x} + \sin(t + \phi_0) \frac{\partial f_{e,p}}{\partial p_y} \\ = \frac{\sin \psi}{p^2} \frac{\partial g_{e,p}}{\partial \psi} - \cos \psi \frac{\partial}{\partial p} \frac{g_{e,p}}{p}. \end{aligned} \quad (24)$$

Then, from Eqs. (17) and (18) we have:

$$\begin{aligned} \frac{\partial g_{e,p}}{\partial t} &= -\frac{\partial g_{e,p}}{\partial \psi} \pm \frac{\sin \psi}{p} \frac{\partial g_{e,p}}{\partial \psi} \mp p \cos \psi \frac{\partial}{\partial p} \frac{g_{e,p}(p, \psi)}{p} + \\ & \int_p^\infty g_\gamma(p', \psi) \tilde{w}(p' \rightarrow p, \psi) dp' + \\ & \int_p^\infty g_{e,p}(p', \psi) w(p' \rightarrow p, \psi) dp' - W g_{e,p}, \end{aligned} \quad (25)$$

$$\begin{aligned} \frac{\partial g_\gamma}{\partial t} &= -\frac{\partial g_\gamma}{\partial \psi} - \tilde{W} g_\gamma + \\ & \int_p^\infty [g_e(p', \psi) + g_p(p', \psi)] w(p' \rightarrow p' - p, \psi) dp', \end{aligned} \quad (26)$$

where $g_{e,p,\gamma}$, W and \tilde{W} are defined at the point (p, ψ) . The probability rates w , \tilde{w} contained in Eqs. (25), (26) can be found in the framework of the quasiclassical theory [11, 29]:

$$\begin{aligned} w(\mathbf{p}' \rightarrow \mathbf{p}) &= -\frac{\alpha}{\varepsilon_l a_0} \frac{1}{p'^2} \left[\int_{\varkappa}^\infty \text{Ai}(\xi) d\xi + \right. \\ & \left. \left(\frac{2\eta^{2/3}}{(1-\eta)^{2/3}} + \frac{(1-\eta)^{4/3}}{\eta^{1/3}} \right) \chi'^{2/3} \text{Ai}'(\varkappa) \right], \end{aligned} \quad (27)$$

$$\begin{aligned} \tilde{w}(\mathbf{p}' \rightarrow \mathbf{p}) &= \frac{\alpha}{\varepsilon_l a_0} \frac{1}{p'^2} \left[\int_{\tilde{\varkappa}}^\infty \text{Ai}(\xi) d\xi + \chi'^{2/3} \text{Ai}'(\tilde{\varkappa}) \right. \\ & \left. \times \left(2\eta^{2/3} (1-\eta)^{2/3} - \frac{1}{\eta^{1/3} (1-\eta)^{1/3}} \right) \right], \end{aligned} \quad (28)$$

where

$$\varkappa = \left(\frac{1-\eta}{\eta \chi'} \right)^{2/3}, \quad (29)$$

$$\tilde{\varkappa} = \left(\frac{1}{\eta(1-\eta)\chi'} \right)^{2/3}, \quad (30)$$

$\eta = p/p'$, $\chi' = \varepsilon_l a_0^2 p' \sin \psi$ is the quantum parameter for the initial particle, $\varepsilon_l = \hbar \omega_l / mc^2$ is the frequency of the field rotation in Compton units, $\alpha = e^2 / \hbar c$ is the fine structure constant, $\text{Ai}(\xi)$ and $\text{Ai}'(\xi)$ are the Airy function and its derivative, respectively [43]. Eqs. (25)-(28) are the complete set of equations which describes evolution of the distribution functions in the momentum space for the electromagnetic cascade in the rotating electric field.

IV. SCALABILITY OF THE CASCADE EQUATIONS

Eqs. (25) and (26) governing cascade dynamics depend on two parameters: period of the electric field rotation

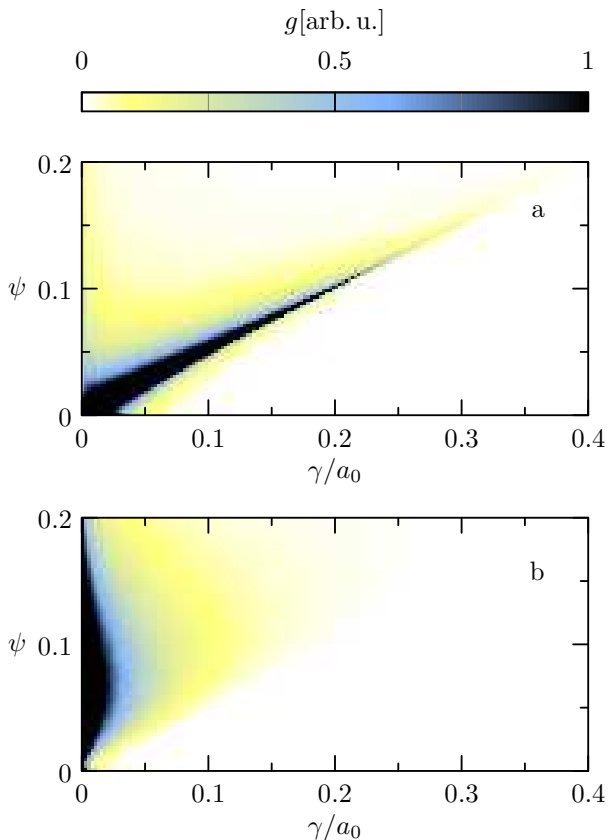


Figure 2: The distribution functions of (a) the electrons and (b) the photons of the electromagnetic cascade developing in the rotating electric field with the normalized amplitude $a_0 = 1.6 \times 10^9$ and $\lambda_l = 0.8 \mu\text{m}$.

and the field strength. However, it can be shown that if $E_0 \gg \alpha E_{cr}$ the number of the parameters can be reduced. It is shown in Ref. [37] that if $E_0 \gg \alpha E_{cr}$ and $\lambda_l \gtrsim 2\pi\hbar/mc\alpha^2 \approx 50 \text{ nm}$ the characteristic time between consecutive photon emissions by the cascade electron (positron) are much smaller than the period of the electric field rotation $2\pi/\omega_l$. In other words, the number of the cascade particles increases in many times during the period of the electric field rotation, $\Gamma \gg 1$, where Γ is the cascade growth rate normalized to ω_l . The number of cascade particles increases exponentially $N \propto \exp(\Gamma t)$.

The simplification of the kinetic equations and the reduction of the number of the governing parameters are possible due to the fact that in this case the cascade particles are concentrated in the regions $|\sin \psi| \ll 1$. As we will see later it follows from numerical simulations that the condition $|\sin \psi| \ll 1$ holds for the most of the particles produced in the cascade. This can be qualitatively explained as follows. Eq. (10) implies that $p \sim 1$ achieves when the electrons or positrons are accelerated within the time interval about the period of the electric field rotation. If $E_0 \gg \alpha E_{cr}$, the electron emits a lot of photons within this time interval and loses a great part of the gained energy. Hence, the electron does not gain high

energy from the field and its characteristic momentum is small $p \ll 1$. In accordance with Eq. (9), the angle ψ between the electron velocity and the direction opposite to the electric field direction, changes very quickly until $|\sin \psi| \lesssim p \ll 1$. The photons emitted by the electrons mostly have $|\sin \psi| \ll 1$. Furthermore, for the photons $d\psi/dt = 1$, so they decay before the angle ψ changes significantly. Therefore, it is natural to assume that the distribution functions of the electrons, the positrons and the photons are substantially nonzero only in the region $|\sin \psi| \ll 1$.

Using the fact that $|\sin \psi| \ll 1$, the kinetic equations can be simplified as follows. $|\sin \psi| \ll 1$ if $\psi \approx 0$ or $\psi \approx \pi$. Let us, for the specificity, consider the region $|\psi| \ll 1$. In this region the following substitutions can be made in Eq. (25): $\cos \psi \rightarrow 1$, $\sin \psi \rightarrow \psi$. In the resulting equation as well as in Eq. (26) (with probabilities from Eqs. (27), (28)) the following substitution

$$t = \beta \hat{t}, \quad (31)$$

$$p = \beta \hat{p}, \quad (32)$$

$$\psi = \beta \hat{\psi} \quad (33)$$

does not change anything except parameter $\chi \approx \varepsilon_l a_0^2 p \psi = \varepsilon_l a_0^2 \beta^2 \hat{p} \hat{\psi}$, where β is arbitrary quantity. Choosing

$$\beta = \frac{1}{\varepsilon_l^{1/2} a_0}, \quad (34)$$

yields $\chi = \hat{p} \hat{\psi}$. The resulting equations for the distribution functions depend only on the parameter

$$\mu = \frac{\varepsilon_l a_0}{\alpha} = \frac{1}{\alpha} \frac{E_0}{E_{cr}}. \quad (35)$$

They do not depend on the frequency ω_l and, hence, on the corresponding wavelength $\lambda_l = 2\pi c/\omega_l$. Thus, the dependence of various cascade characteristics on λ_l is determined only by the scaling Eqs. (31)-(34). For example, it follows from Eq. (31) that for the certain field amplitude and, hence, the intensity $I = cE_0^2/4\pi$, the growth rates at two different wavelengths relates as follows:

$$\frac{\Gamma(I, \lambda_{l,1})}{\Gamma(I, \lambda_{l,2})} = \sqrt{\frac{\lambda_{l,1}}{\lambda_{l,2}}}. \quad (36)$$

This formula is in good agreement with the results of the numerical simulations as shown in Sec. VII.

V. SCALABILITY OF THE KINETIC EQUATIONS FOR PARTICLES WITH $\chi \gg 1$

Further simplification can be made if we consider high-energy "tails" of the distribution functions with $\chi \gg 1$. This let us to simplify the formulae for the spectral distributions of the probabilities Eq. (27), (28). First, in the

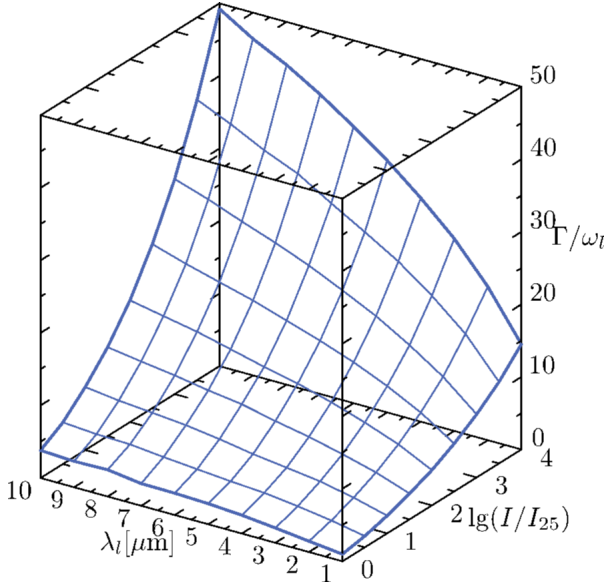


Figure 3: The growth rate of the electromagnetic cascade in the rotating electric field as a function of $I = cE_0^2/4\pi$ and $\lambda_l = 2\pi c/\omega_l$. Here E_0 is the amplitude of the electric field, ω_l is the cyclic frequency of the field rotation, $I_{25} = 10^{25}$ W/cm².

region where the probabilities are substantially nonzero, the derivative and the integral of the Airy function are of the same order: $\int_{\varkappa}^{\infty} \text{Ai}(\xi) d\xi \sim \text{Ai}'(\varkappa)$ if $0 < \varkappa \lesssim 1$. Second,

$$\min \left\{ \frac{2\eta^{2/3}}{(1-\eta)^{2/3}} + \frac{(1-\eta)^{4/3}}{\eta^{1/3}} \right\} \approx 2, \quad (37)$$

$$\min \left\{ \frac{1}{\eta^{1/3}(1-\eta)^{1/3}} - 2\eta^{2/3}(1-\eta)^{2/3} \right\} \approx 0.8, \quad (38)$$

if $\eta \in (0, 1)$. Hence, as soon as $\chi \gg 1$, the terms in Eqs. (27) and (28) that are proportional to the integrals of the Airy function can be neglected. Furthermore, \varkappa is much smaller than unity on a wide interval $1/\chi' \ll \eta \leq 1$, and $\tilde{\varkappa} \ll 1$ if $1/\chi' \ll \eta$ and $1-\eta \gg 1/\chi'$. Then in Eqs. (27) and (28) we can set $\varkappa = \tilde{\varkappa} = 0$. However, this lead to appearing of the singularities in the expressions for w and \tilde{w} , namely $w \propto 1/\eta^{1/3}$ at $\eta \rightarrow 0$, $\tilde{w} \propto 1/\eta^{1/3}$ if $\eta \rightarrow 0$ and $\tilde{w} \propto 1/(1-\eta)^{1/3}$ if $\eta \rightarrow 1$. Nevertheless, these singularities are integrable and give contributions to the total probability rates that are about $\chi'^{2/3} \gg 1$ times smaller than the total probability rates.

Finally, for $\chi' \gg 1$ and $|\psi| \ll 1$ we have:

$$w(\mathbf{p}' \rightarrow \mathbf{p}) = -\text{Ai}'(0) \frac{\alpha a_0^{1/3} \psi^{2/3}}{\varepsilon_l^{1/3} p^{4/3}} \frac{1+\eta^2}{\eta^{1/3}(1-\eta)^{2/3}}, \quad (39)$$

$$\tilde{w}(\mathbf{p}' \rightarrow \mathbf{p}) = -\text{Ai}'(0) \frac{\alpha a_0^{1/3} \psi^{2/3}}{\hbar^{1/3} p^{4/3}} \frac{\eta^2 + (1-\eta)^2}{\eta^{1/3}(1-\eta)^{1/3}}, \quad (40)$$

$$W(p', \psi) = v \frac{\alpha a_0^{1/3} \psi^{2/3}}{\varepsilon_l^{1/3} p^{1/3}}, \quad (41)$$

and the same expression for \tilde{W} except substitution \tilde{v} for v , where

$$v = -\text{Ai}'(0) \int_0^1 \frac{1+\eta^2}{\eta^{1/3}(1-\eta)^{2/3}} d\eta \approx 1.46, \quad (42)$$

$$\tilde{v} = -\text{Ai}'(0) \int_0^1 \frac{\eta^2 + (1-\eta)^2}{\eta^{1/3}(1-\eta)^{1/3}} d\eta \approx 0.38. \quad (43)$$

Furthermore, Eq. (26) can be used in the same form and Eq. (25) can be simplified as follows:

$$\begin{aligned} \frac{\partial g_{e,p}}{\partial t} = & -\frac{\partial g_{e,p}}{\partial \psi} \pm \frac{\psi}{p} \frac{\partial g_{e,p}}{\partial \psi} \mp p \frac{\partial}{\partial p} \frac{g_{e,p}}{p} + \\ & \int_p^\infty g_\gamma(p', \psi) \tilde{w}(p' \rightarrow p, \psi) dp' + \\ & \int_p^\infty g_{e,p}(p', \psi) w(p' \rightarrow p, \psi) dp' - W g_{e,p}. \end{aligned} \quad (44)$$

Similar equations can be written in the region $\chi \gg 1$, $|\psi - \pi| \ll 1$.

The substitution:

$$t = \frac{\varepsilon_l^{1/4}}{\alpha^{3/4} a_0^{1/4}} \bar{t}, \quad (45)$$

$$\psi = \frac{\varepsilon_l^{1/4}}{\alpha^{3/4} a_0^{1/4}} \bar{\psi}, \quad (46)$$

$$p = \frac{\varepsilon_l^{1/4}}{\alpha^{3/4} a_0^{1/4}} \bar{p}. \quad (47)$$

in Eqs. (26), (39)-(44) yields the following parameter-free equations:

$$\begin{aligned} \frac{\partial g_{e,p}}{\partial \bar{t}} = & -\frac{\partial g_{e,p}}{\partial \bar{\psi}} \pm \frac{\bar{\psi}}{\bar{p}} \frac{\partial g_{e,p}}{\partial \bar{\psi}} \mp \bar{p} \frac{\partial}{\partial \bar{p}} \frac{g_{e,p}}{\bar{p}} + \\ & \int_{\bar{p}}^\infty g_\gamma(\bar{p}', \bar{\psi}) \bar{w}_\gamma(\bar{p}' \rightarrow \bar{p}, \bar{\psi}) d\bar{p}' + \\ & \int_{\bar{p}}^\infty g_{e,p}(\bar{p}', \bar{\psi}) \bar{w}(\bar{p}' \rightarrow \bar{p}, \bar{\psi}) d\bar{p}' - \bar{W} g_{e,p}, \end{aligned} \quad (48)$$

$$\begin{aligned} \frac{\partial g_\gamma}{\partial \bar{t}} = & -\frac{\partial g_\gamma}{\partial \bar{\psi}} - \bar{W}_\gamma g_\gamma + \\ & \int_{\bar{p}}^\infty [g_e(\bar{p}', \bar{\psi}) + g_p(\bar{p}', \bar{\psi})] \bar{w}(\bar{p}' \rightarrow \bar{p}', \bar{\psi}) d\bar{p}', \end{aligned} \quad (49)$$

where

$$\bar{w}(\bar{p}' \rightarrow \bar{p}) = -\text{Ai}'(0) \frac{\bar{\psi}^{2/3}}{\bar{p}'^{4/3}} \frac{1+\eta^2}{\eta^{1/3}(1-\eta)^{2/3}}, \quad (50)$$

$$\bar{w}_\gamma(\bar{p}' \rightarrow \bar{p}) = -\text{Ai}'(0) \frac{\bar{\psi}^{2/3}}{\bar{p}'^{4/3}} \frac{\eta^2 + (1-\eta)^2}{\eta^{1/3}(1-\eta)^{1/3}}, \quad (51)$$

$$\bar{W}(\bar{p}, \bar{\psi}) = v \frac{\bar{\psi}^{2/3}}{\bar{p}^{1/3}}, \quad (52)$$

$$\bar{W}_\gamma(\bar{p}, \bar{\psi}) = \tilde{v} \frac{\bar{\psi}^{2/3}}{\bar{p}^{1/3}}, \quad (53)$$

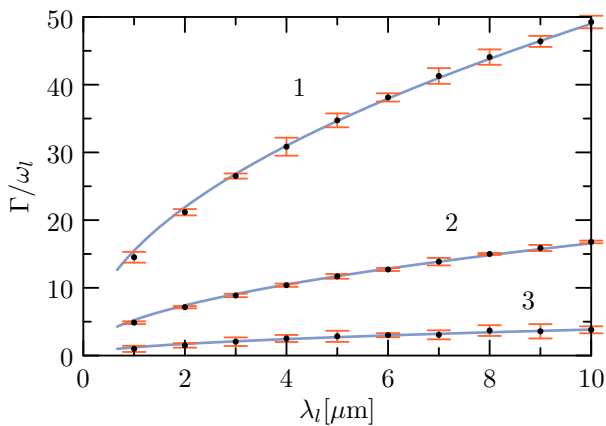


Figure 4: The dependence of the growth rate on λ_l : the numerical data (dots) and the fits $\Gamma/\omega_l = A\sqrt{\lambda_l}$ for the data (lines). The amplitude A is chosen such that the RMS deviation from the numerical data is minimal. The error bars show the dispersion of the numerical data for 7 runs of the simulation. Line 1 corresponds to the data obtained for $I = 10^{29}$ W/cm², line 2 corresponds to $I = 10^{27}$ W/cm² and line 3 corresponds to $I = 10^{25}$ W/cm².

The obtained equations can be used for further analysis of the particle distribution during the cascade development. However, these equations do not completely determine the cascade dynamics, because they describe only the particles with high χ . For example, the particles with $\chi \sim 1$ can also breed and give some contribution to the growth rate.

Let us assume that the growth rate is determined only by the particles with $\chi \gg 1$, $|\psi| \ll 1$ and $|\psi - \pi| \ll 1$. In this case the dependence of Γ on the electric field strength and the wavelength can be determined from Eq. (45) as follows:

$$\frac{\Gamma(\mu_1, \lambda_{l,1})}{\Gamma(\mu_2, \lambda_{l,2})} = \frac{\mu_1^{1/4} \lambda_{l,1}^{1/2}}{\mu_2^{1/4} \lambda_{l,2}^{1/2}}, \quad (54)$$

where $\mu = E_0/\alpha E_{cr}$. The dependence Eq. (54) and the scaling Eqs. (45)-(47) was also derived in Ref. [37] via simple estimations and dimensional analysis of the kinetic equations. However, the numerical simulations show that in a wide range of the parameters Eq. (54) is not valid (see Sec. VII and right plot in Fig. 7 in Ref. [37]) and can be used only for estimations with accuracy about 50%. Thus, the growth rate Γ is not completely determined by Eqs. (48)-(53) that describe only particles with $\chi \gg 1$. However, the growth rate contributes to these equations through time derivatives. Hence, for further analysis of Eqs. (48)-(49) we assume that Γ is known (for example, from the numerical simulations).

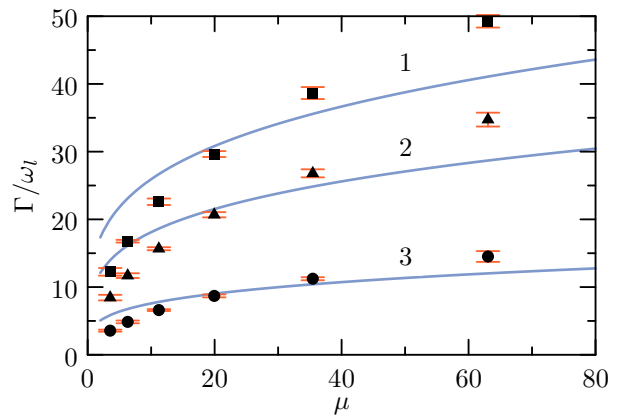


Figure 5: The dependence of the growth rate on $\mu = E_0/\alpha E_{cr}$. The numerical results are presented by the solid black dots. The error bars show the dispersion of the numerical data for 7 runs of the simulation. The solid lines represent fits $\Gamma = A\mu^{1/4}$. The amplitude A is chosen such that the RMS deviation from the numerical data is minimal. Line 1 corresponds to numerical data for $\lambda_l = 10$ μm (squares), line 2 corresponds to $\lambda_l = 5$ μm (triangles) and line 3 corresponds to $\lambda_l = 1$ μm (circles).

VI. ANALYTICAL SOLUTIONS AND ENERGY SPECTRA

Here we again restrict ourselves to the limit $E_0 \gg \alpha E_{cr}$, and consider the "tails" of the distribution functions that correspond to $\chi \gg 1$ and, additionally, to $p \gg \langle p \rangle$ in order to estimate the terms in Eqs. (48), (49) and obtain approximate solutions for the stationary particle distribution functions as well as for the energy spectra of the electrons, the positrons and the photons. Here $\langle p \rangle$ is the average particle momentum and the stationary distribution means that the distribution function shape is approximately conserved during the evolution, but the number of particles grows exponentially:

$$g_{e,p,\gamma} \propto \exp(\Gamma t), \quad (55)$$

$$\frac{\partial g_{e,p,\gamma}}{\partial t} = \Gamma g_{e,p,\gamma}. \quad (56)$$

The numerical simulations show that the distribution functions approach such dependence in time interval about some $1/\Gamma$ after the cascade starts.

The main source of the electrons with $|\psi| \ll 1$, $p \gg \langle p \rangle$ is their transfer from the region $p \lesssim \langle p \rangle$ due to the acceleration. So, electrons are concentrated along the separatrix $\psi \approx p/2$ owing to the phase flow. We will see that the ψ -width of the electron distribution function at $p \gg \langle p \rangle$ is much smaller than the angular width of the photon distribution function and much smaller than p . Because of that we derive the electron energy spectrum and do not derive the angular shape of the electron distribution function.

Furthermore, we will show that particle spectra

$$h_{e,p,\gamma}(p) = \int_0^{2\pi} g_{e,p,\gamma}(p, \psi) d\psi \quad (57)$$

decrease exponentially with the increase of p due to transfer of the electrons with high momenta to the region of lower momenta because of frequent emission of the photons. Besides, the characteristic scale of the decrease is less or about the average momentum $\langle p \rangle$. Hence, the electrons that acquire momentum p due to the photon emission mostly have momentum p' before the emission in the following narrow interval: $p < p' \lesssim p + \langle p \rangle$. The electrons that initially have momentum p are distributed on wide interval $p' \in (0, p)$ with the average momentum about p after the photon emission, because the characteristic p' -scale of the function $w(\mathbf{p} \rightarrow \mathbf{p}')$ is the same order as p . The last two terms in Eq. (48) describe the photon emission. The last but one term in Eq. (48) describes the inflow of the electrons from the region of high momenta $p' > p$, and the last term describes the outflow of the electrons to the region of momenta less than p . Summarizing, we obtain that the last but one term is about $p/\langle p \rangle \gg 1$ times smaller than the last term and can be described in the framework of the perturbation theory. It can be shown by similar reasoning that the term with g_γ in Eq. (48) can be neglected.

Integrating Eq. (48) for the electrons over the interval $\bar{\psi} \in (\bar{p}/2 - \Delta\bar{\psi}, \bar{p}/2 + \Delta\bar{\psi})$, where $\Delta\bar{\psi} \ll \bar{p}/2$ and much higher than the ψ -width of the electron distribution function, and neglecting g_γ , we obtain:

$$\frac{\partial h_e}{\partial \bar{p}} = -\bar{\Gamma} h_e - \frac{v\bar{p}^{1/3}}{2^{2/3}} h_e - 2^{1/3} \text{Ai}'(0) \bar{p}^{1/3} \int_0^\infty \frac{h_e(\bar{p}[1 + \xi])}{\xi^{2/3}} d\xi, \quad (58)$$

where we simplify the formula for $\bar{w}(p' \rightarrow p, \psi)$ taking into account that $\psi \approx p'/2$ and $p' - p \sim \langle p \rangle \ll p$. As it was already mentioned, the characteristic scale of the integrand in the last term of Eq. (58) is $\xi \sim \langle p \rangle/p \ll 1$ and this term can be treated as perturbation. In the zeroth order of the perturbation theory we have:

$$h_e(\bar{p}) = h_0 \exp \left[-\bar{\Gamma} \bar{p} - \frac{3v\bar{p}^{4/3}}{2^{8/3}} \right], \quad (59)$$

where h_0 is a constant. Then, using the following approximation derived by the expansion of the terms in the exponent in Tailor series

$$h_e(\bar{p}[1 + \xi]) \approx h_e(\bar{p}) \exp \left[- \left(\bar{\Gamma} \bar{p} + \frac{v\bar{p}^{4/3}}{2^{2/3}} \right) \xi \right]. \quad (60)$$

we obtain:

$$\frac{1}{h_e} \frac{\partial h_e}{\partial \bar{p}} = -\bar{\Gamma} - \frac{v\bar{p}^{1/3}}{2^{2/3}} - \frac{2^{1/3} \text{Ai}'(0) b_{-2/3}}{[\bar{\Gamma} + v\bar{p}^{1/3}/2^{2/3}]^{1/3}}, \quad (61)$$

where

$$b_i = \int_0^\infty \xi^i \exp(-\xi) d\xi, \quad (62)$$

and $b_{-2/3} \approx 2.68$. Finally, from Eq. (61) we have:

$$h_e(\bar{p}) = h_0 \exp \left\{ -\bar{\Gamma} \bar{p} - \frac{3v\bar{p}^{4/3}}{2^{8/3}} - \frac{9 \text{Ai}'(0) b_{-2/3} \bar{\Gamma}^{8/3}}{5 \times 2^{2/3} v^3} \times \left[(\mathbf{p}^{1/3} + 1)^{2/3} (5\mathbf{p}^{2/3} - 6\mathbf{p}^{1/3} + 9) - 9 \right] \right\}, \quad (63)$$

where $\mathbf{p} = v^3 \bar{p} / 4\bar{\Gamma}^3$.

The positrons are decelerated in the region $|\psi| \ll 1$, so, the only source of the photons in the region $|\psi| \ll 1$, $p \gg \langle p \rangle$ are the electrons, hence, we can neglect g_p and assume $\bar{p}' - \bar{p} \ll \bar{p}'$ in Eq. (49), that yield:

$$\frac{\partial g_\gamma}{\partial \bar{\psi}} = -\bar{\Gamma} g_\gamma - \frac{\tilde{v} \bar{\psi}^{2/3}}{\bar{p}^{1/3}} g_\gamma - \frac{2^{1/3} \text{Ai}'(0) h_e(2\bar{\psi})}{\bar{p}^{1/3} (2\bar{\psi} - \bar{p})^{1/3}}. \quad (64)$$

In order to obtain this equation we also use the electron distribution function in the following form:

$$g_e(\bar{p}', \bar{\psi}) = h_e(\bar{p}') \delta(\bar{\psi} - \bar{p}'/2), \quad (65)$$

where $\delta(x)$ is the Dirac delta function. Obviously, the photons, emitted by the electrons in the region $|\psi| \ll 1$, are situated in the $p - \psi$ space above the line $\psi = p/2$. As far as we assume that the photons decay before they pass the distance about π along ψ -direction, we can set $g_\gamma(\bar{p}, \bar{p}/2) = 0$. Additionally, making of use the following approximations in the solution of Eq. (64)

$$h_e(2\bar{\psi}) \approx h_e(\bar{p}) \exp \left[- \left(\bar{\Gamma} + \frac{v\bar{p}^{1/3}}{2^{2/3}} \right) (2\bar{\psi} - \bar{p}) \right], \quad (66)$$

$$\bar{\psi}^{5/3} - \left(\frac{\bar{p}}{2} \right)^{5/3} \approx \frac{5\bar{p}^{2/3}}{3 \times 2^{2/3}} \left(\bar{\psi} - \frac{\bar{p}}{2} \right), \quad (67)$$

we obtain for $\bar{p}/2 < \bar{\psi} \ll 1$:

$$g_\gamma(\bar{p}, \bar{\psi}) = - \frac{\text{Ai}'(0) h_e(\bar{p})}{\bar{p}^{1/3} [\bar{\Gamma} + (2^{1/3} v - \tilde{v}/2^{2/3}) \bar{p}^{1/3}]^{2/3}} \times \int_0^\varphi \frac{\exp(-\xi)}{\xi^{1/3}} d\xi \times \exp \left[-\bar{\Gamma} \left(\bar{\psi} - \frac{\bar{p}}{2} \right) - \frac{3\tilde{v}}{5\bar{p}^{1/3}} \left(\bar{\psi}^{5/3} - \frac{\bar{p}^{5/3}}{2^{5/3}} \right) \right], \quad (68)$$

where

$$\varphi = \left[\bar{\Gamma} + \left(2^{1/3} v - \tilde{v}/2^{2/3} \right) \bar{p}^{1/3} \right] (\psi - \bar{p}/2). \quad (69)$$

Further simplifications can be made if we assume that $2^{1/3} v \bar{p}^{1/3} \gg \bar{\Gamma}$ and take into account that $\tilde{v}/v \approx 0.26 \ll 1$. In this case the characteristic scale of the integral in Eq. (68) is much smaller than the scale of the exponent in

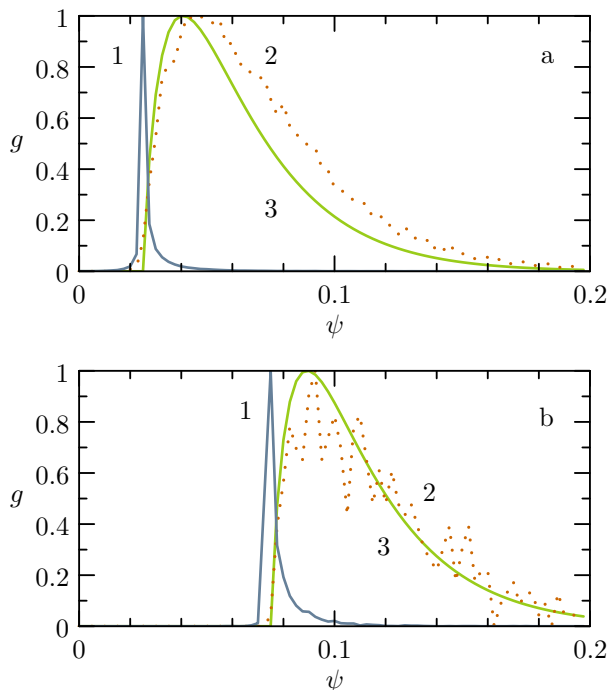


Figure 6: The electron (line 1) and the photon (line 2) distribution functions obtained by the numerical simulation of the electromagnetic cascade developing in the rotating electromagnetic field with $a_0 = 8 \times 10^5$ and $\lambda_l = 0.8 \mu\text{m}$ for γ : $\gamma/a_0 = 0.05$ (a) and $\gamma/a_0 = 0.15$ (b). Lines 3 correspond to the analytical expression for the photon distribution function Eq. (68). All plotted functions are normalized to their maximal values.

Eq. (68). Thus, integrating Eq. (68) over ψ , we assume that the integral in this equation is equal to its maximal value $b_{-1/3}$ if $\varphi > 0$. We also suppose that the positron distribution function concentrated generally near $\psi = \pi$ gives the same photon distribution as Eq. (68) except the substitution $\psi - \pi$ for ψ . Furthermore, in order to advance simplification we can use Taylor's expansion in the exponent of Eq. (68) similarly to Eqs. (66) and (67). Finally we obtain the following expression for the photon energy spectrum:

$$h_\gamma(\bar{p}) = -\frac{2 \text{Ai}'(0) b_{-1/3} h_e(\bar{p})}{\bar{p}^{1/3} [\bar{\Gamma} + (2^{1/3} v - \tilde{v}/2^{2/3}) \bar{p}^{1/3}]^{2/3}} \times \frac{1}{[\bar{\Gamma} + \tilde{v} \bar{p}^{1/3}/2^{2/3}]}. \quad (70)$$

VII. NUMERICAL SIMULATIONS

In this section we compare the analytical expressions for the electron energy spectrum (63), the photon energy spectrum (70) and for the photon distribution function (68) with the results obtained using the numerical model described in Ref. [28]. Furthermore, using the nu-

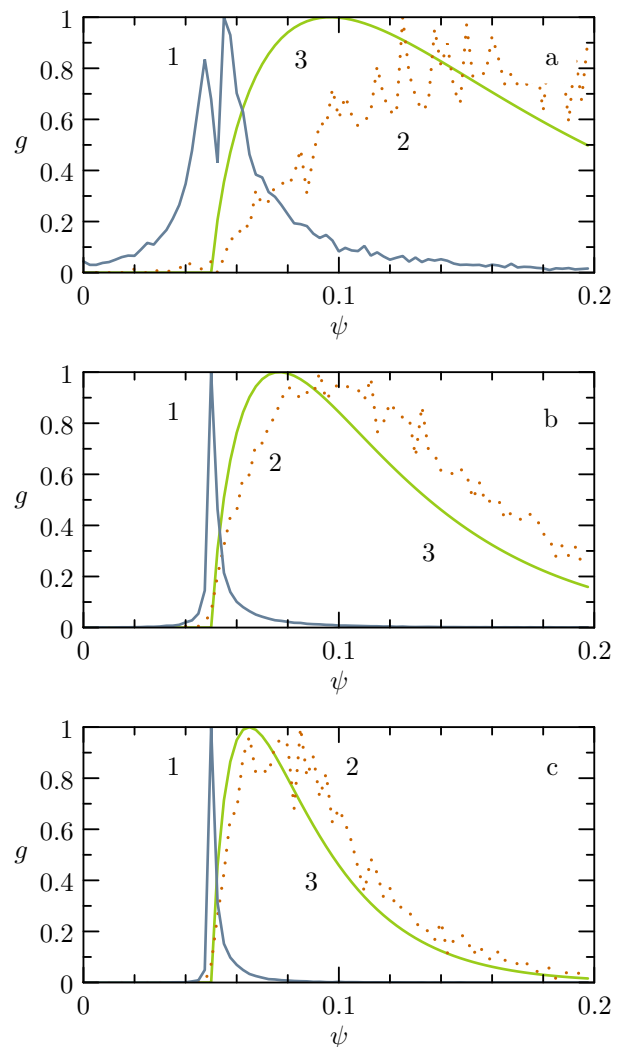


Figure 7: The electron (line 1) and the photon (line 2) distribution functions at $\gamma/a_0 = 0.1$ obtained by the numerical simulations of the electromagnetic cascade developing in the rotating electromagnetic field with $\lambda_l = 0.8 \mu\text{m}$ and (a) $a_0 = 3.2 \times 10^4$, (b) $a_0 = 1.6 \times 10^5$, (c) $a_0 = 8 \times 10^5$. Lines 3 correspond to the analytical expression for the photon distribution function Eq. (68). All plotted functions are normalized to their maximal values.

merical values of $\bar{\Gamma}$, we compare various terms in these expressions and simplify them for a wide range of parameters.

The electron and the photon distribution functions in electromagnetic cascade are shown in Fig. 2. These functions are obtained in the numerical simulation performed for the field parameters $a_0 = 1.6 \times 10^5$, $\lambda_l = 0.8 \mu\text{m}$. The numerical simulation gives $\Gamma/\omega_l \approx 12.1$ for these parameters. The shape of the distribution functions is typical for the cascades with $\Gamma \gg 1$. The electron distribution function at $p \gg \langle p \rangle$ is concentrated near the line $\psi = p/2$, and the photon distribution function is nonzero upper this line, that agrees well with the qualitative description given in Sec. VI. Furthermore, it follows from Fig. 2

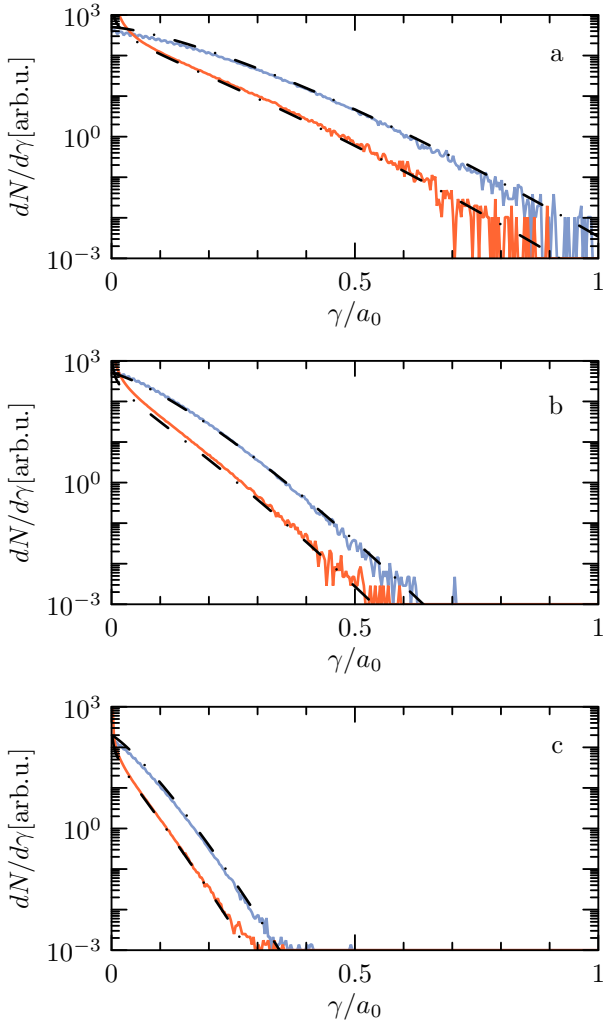


Figure 8: The electron (upper lines) and the photon (lower lines) energy spectra for the electromagnetic cascade developing in the rotating electric field with $\lambda_l = 0.8 \mu\text{m}$ and (a) $a_0 = 3.2 \times 10^4$, (b) $a_0 = 1.6 \times 10^5$, (c) $a_0 = 8 \times 10^5$. Solid lines correspond to the numerical results and the dash-dotted lines correspond to the analytical expressions (63) and (70).

and the results of the numerical simulation that almost all particles are located in the regions $p \ll 1$, $|\psi| \ll 1$ and $p \ll 1$, $|\psi - \pi| \ll 1$.

The dependence of the growth rate Γ on the electric field parameters is shown on Fig. 3. In every node of the surface Γ is calculated 7 times and the result is averaged out. It is seen that Γ grows with the increase of the intensity and the wavelength, and the growth of Γ due to the wavelength increase is much steeper than the growth due to the intensity increase. Therefore, it is preferable to use longer wavelengths in the experiments devoting to the cascades observation. Besides, the limitation of the attainable intensity due to prolific pair production is less strict for shorter wavelengths.

In Fig. 4 the dependence of the growth rate on the wavelength for three different values of the intensity is

shown. The rows of dots show the results of the numerical simulations. The error bars show the dispersion of Γ obtained for 7 simulations with the same initial parameters. The cascades in the simulations are initiated by a single immobile e^+e^- pair. Thus, at initial stage of the cascade development when the number of cascade particles is small the shape of the distribution functions is being modified. Because of this the growth rate fluctuates significantly at the initial stage. We measure the growth rate as $\Gamma = d(\ln N_e)/dt$ at the later stage of the cascade development when the number of particles is high and the growth rate becomes constant. The dispersion of Γ , obtained in the simulations, is explained by the finiteness of the particle number used in the simulations. The solid lines in Fig. 4 are the fits described by the equation $\Gamma = A\sqrt{\lambda_l}$, where A is chosen for every row of the numerical data such that the RMS difference between the numerical data and the fit is minimal. The line 1 corresponds to the numerical data obtained for $I = 10^{29} \text{ W/cm}^2$, the line 2 corresponds to the numerical data obtained for $I = 10^{27} \text{ W/cm}^2$ and the line 3 corresponds to the numerical data obtained for $I = 10^{25} \text{ W/cm}^2$. It is seen from Fig. 4 that the theoretically obtained dependence of the growth rate on the wavelength Eq. (36) is in good agreement with the results of the numerical simulations.

The dependence of the growth rate on the electric field strength is shown in Fig. 5. Black points present the results of the numerical simulations, and the solid lines are the RMS fits $\Gamma = A\mu^{1/4}$ that correspond to Eq. (54). The line 1 corresponds to the squares that illustrate the numerical results obtained for $\lambda_l = 10 \mu\text{m}$, the line 2 belongs to the triangles that illustrate the numerical data for $\lambda_l = 5 \mu\text{m}$ and the line 3 corresponds to the numerical data obtained for $\lambda_l = 1 \mu\text{m}$ (circles). It follows from Fig. 5 that Eq. (54) can be used only for estimations of Γ with accuracy about 50%. However, Eq. (54) is derived under the assumption that $\chi \gg 1$ for the most of cascade particles, but actually many cascade particles can have $\chi \sim 1$. These particles can give substantial contribution to the cascade dynamics and, hence, to the cascade growth rate. Indeed, numerical simulations show that for $I = 10^{27} \text{ W/cm}^2$, $\lambda_l = 1 \mu\text{m}$ the portion of the electrons with $\chi < 5$ is about 30% and this portion for $I = 10^{25} \text{ W/cm}^2$, $\lambda_l = 1 \mu\text{m}$ is about 90%.

The comparison between Eq. (68) and $g_{ph}(\psi)$ at certain value of p obtained by the numerical simulations is given in Fig. 6. The line 1 and the line 2 correspond to the electron and the photon distribution functions, respectively. The line 3 corresponds to the solution (68). The distribution functions are normalized to their maximal values. The parameters of the electric field are: $a_0 = 8 \times 10^5$, $\lambda_l = 0.8 \mu\text{m}$. The distribution functions $g_{e,\gamma}(\psi, p)$ are shown at $p = 0.05$ (plate a) and at $p = 0.15$ (plate b). The growth rate used in Eq. (68) is calculated numerically: $\Gamma/\omega_l = 24.1$. It is seen that the electron distribution function is much narrower than that of the photons. Furthermore, the numerical results are in good

agreement with Eq. (68). Similar cuts of the distribution functions are shown in Fig. 7. The panel (a) corresponds to $a_0 = 3.2 \times 10^4$ and $\Gamma = 6.29$ obtained in the simulation, the panel (b) corresponds to $a_0 = 1.6 \times 10^5$ and $\Gamma = 12.1$, the panel (c) corresponds to $a_0 = 8 \times 10^5$ and $\Gamma = 24.1$. It is seen from the plates (b) and (c) that Eq. (68) is in good agreement with the results of the numerical simulation. However, the photon distribution function obtained theoretically reaches its maximum earlier than the photon distribution function obtained in numerical simulations. Possible explanation of this small discrepancy is the following. In order to obtain Eq. (68) we assume that the electron distribution function depends on the angle ψ as follows: $g_e(p, \psi) \propto \delta(\psi - p/2)$, however, the numerical simulations show that ψ -width of the electron distribution function is finite and big amount of electrons have ψ slightly higher than $p/2$, hence, the maximum of the photon distribution function is also slightly shifted to the region of higher angles. Besides, for the plate (a) the condition $p \gg \langle p \rangle$ is not fulfilled, the shape of electron distribution function in this case becomes more complex than in the case $p \gg \langle p \rangle$ and Eq. (68) gives rather qualitative approximation for the photon distribution function.

In Fig. 8 the electron and the photon energy spectra are shown. The solid lines correspond to the results of the numerical simulations and the dash-dotted lines correspond to Eqs. (63) and (70). The top lines correspond to the electron distribution functions and the bottom lines correspond to the photon distribution functions. In Eqs. (63) and (70) we use Γ from numerical simulations. $\lambda_l = 0.8 \mu\text{m}$, plate (a): $a_0 = 3.2 \times 10^4$, $\Gamma = 6.29$, plate (b): $a_0 = 1.6 \times 10^5$, $\Gamma = 12.1$, plate (c): $a_0 = 8 \times 10^5$, $\Gamma = 24.1$. It is seen that the obtained analytical results are in good agreement with the results of the numerical simulations.

VIII. FURTHER SIMPLIFICATIONS

The obtained analytical expressions for the particle distribution functions are quite complex. Besides, these expressions contain the growth rate Γ that is not derived in the framework of the presented theory. In this section we compare various terms in the obtained expressions and derive asymptotic ($p \rightarrow \infty$) expressions for the particle spectra that are more simple than Eqs. (63), (70). In order to obtain these asymptotic spectra we keep in Eqs. (63) and (70) only the terms that describe the slope of the logarithmic spectra and the ratio between the electron and the photon energy spectra. The slope and the ratio can be probably measured in the future cascade experiments that allows estimating of the field magnitude in the cascade region and the growth rate. Furthermore, we find the fit for Γ guided by the results of the numerical simulations in a wide range of the parameters ($\lambda_l = 1 - 10 \mu\text{m}$, $I = 10^{25} - 10^{29} \text{ W/cm}^2$).

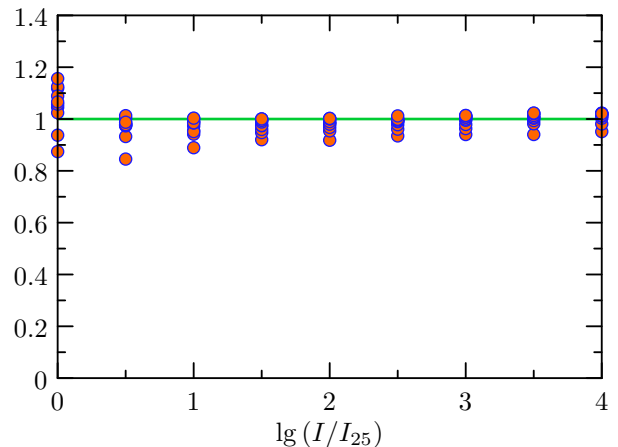


Figure 9: The ratio of the growth rate, Γ , to the fit Eq. (71) (dots) and unity level (line). Γ is computed for the intensity range $I = 10^{25} - 10^{29} \text{ W/cm}^2$ and the range of wavelengths $\lambda = 1 - 10 \mu\text{m}$ with the step $1 \mu\text{m}$.

We can propose the following fit for the growth rate:

$$\Gamma/\omega_l = 0.65 \times \lambda_l^{1/2} [\mu\text{m}] \left(\frac{I}{I_0} \right)^{1/8} \lg \frac{I}{I_0}, \quad (71)$$

where $I_0 = 6 \times 10^{23} \text{ W/cm}^2$, the magnitude and I_0 was chosen in order to obtain good agreement with Γ from the numerical simulations. The ratio of Γ obtained in the numerical simulations of Fig. 3 to the fit Eq. (71) (circles) is shown in Fig. 9. It is seen that Eq. (71) has a satisfactory accuracy.

Making of use Eq. (71) we can estimate the terms in Eqs. (63), (68) and (70). First, for $\bar{\Gamma}$ we obtain the following approximation:

$$\bar{\Gamma} \approx 0.22 \lg \frac{I}{I_0}. \quad (72)$$

Thus, the ratio of the first and the second terms in the exponent in Eq. (63) is

$$\frac{3v\bar{p}^{4/3}}{28^{1/3}\bar{\Gamma}\bar{p}} \approx \frac{3 \times \bar{p}^{1/3}}{\lg I/I_0}. \quad (73)$$

For the considered region of parameters $\lg I/I_0 \approx 1 - 5$. Therefore, asymptotically at high values of \bar{p} this ratio is much more than unity and we can neglect the first term in the exponent in Eq. (63). Besides, the last term in the exponent in Eq. (63) relates to the second term as follows,

$$\frac{0.3}{\bar{\Gamma}^{4/3}\bar{p}^{4/3}} \left[\left(\bar{p}^{1/3} + 1 \right)^{2/3} \times \left(5\bar{p}^{2/3} - 6\bar{p}^{1/3} + 9 \right) - 9 \right], \quad (74)$$

where \bar{p} is introduced right after Eq. (63). This expression decreases with the increase of $\bar{p} \approx 0.8\bar{p}/\bar{\Gamma}^3$, hence,

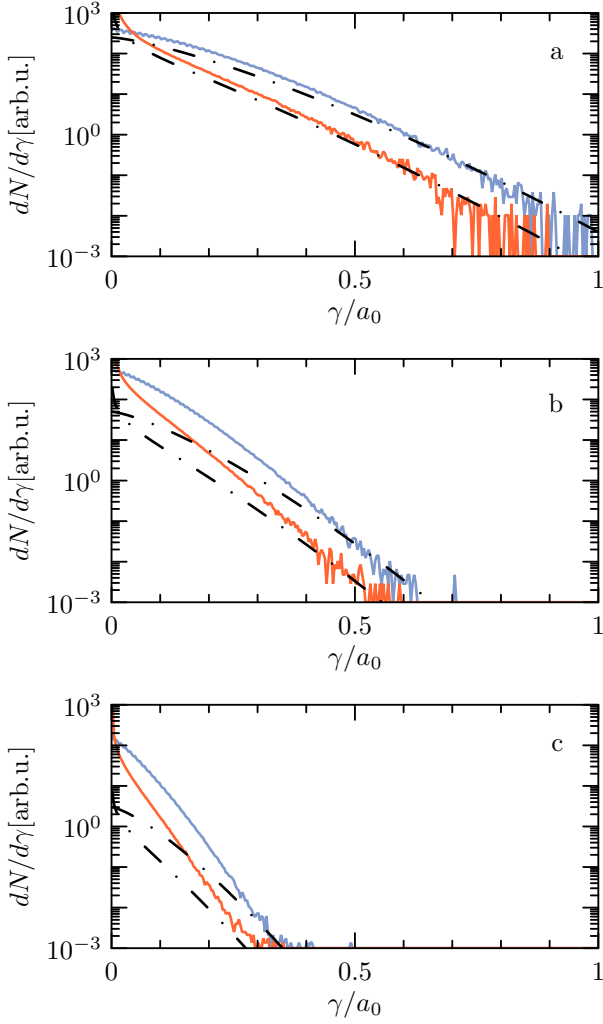


Figure 10: The electron (upper solid lines) and the photon (lower solid lines) energy spectra obtained by the numerical simulations of the electromagnetic cascade developed in the field characterized by $\lambda = 0.8 \mu\text{m}$ and $a_0 = 3.2 \times 10^4$ (plate (a)), $a_0 = 1.6 \times 10^5$ (plate (b)), $a_0 = 8 \times 10^5$ (plate c). The corresponding asymptotic expressions (75) and (77) are shown by the dash-dotted lines.

for sufficiently large values of \bar{p} the last term can be neglected for simplification. Therefore, the electron spectrum Eq. (63) can be reduced to the following asymptotic form:

$$\begin{aligned} h_{e,a}(\gamma) &= h_0 \exp \left[-0.69 \bar{p}^{4/3} \right] \\ &= h_0 \exp \left[-\gamma^{4/3} / \gamma_*^{4/3} \right], \end{aligned} \quad (75)$$

where $\bar{p} = \alpha^{3/4} \varepsilon_l^{-1/4} a_0^{-3/4} \gamma \approx 1.3 \gamma / \gamma_*$ and

$$\gamma_* = 2.4 \times 10^{-7} \lambda_l^{1/2} [\mu\text{m}] I^{3/8} [\text{W}/\text{cm}^2]. \quad (76)$$

In order to simplify Eq. (70) we neglect $\bar{v}/2 \approx 0.19$ in comparison with $v \approx 1.46$ and we neglect $\bar{\Gamma}$ in comparison with $2^{1/3} \bar{v} \bar{p}^{1/3} \approx 1.8 \bar{p}^{1/3}$. However, we does not

neglect $2^{-2/3} \bar{v} \bar{p}^{1/3} \approx 0.24 \bar{p}^{1/3}$ in comparison with $\bar{\Gamma}$. The resulting asymptotic form of the photon spectrum is

$$h_{\gamma,a}(\gamma) = \frac{0.47 h_{e,s}(\gamma)}{\bar{p}^{5/9} [\bar{\Gamma} + 0.24 \bar{p}^{1/3}]}, \quad (77)$$

where

$$\begin{aligned} \bar{\Gamma} &= \varepsilon_l^{1/4} \alpha^{-3/4} a_0^{-1/4} \Gamma / \omega_l \\ &\approx \frac{323}{\lambda_l^{1/2} [\mu\text{m}] I^{1/8} [\text{W}/\text{cm}^2]} \frac{\Gamma}{\omega_l}. \end{aligned} \quad (78)$$

The comparison of Eqs. (75) and (77) with the results of the numerical simulations is given in Fig. 10.

IX. SUMMARY AND DISCUSSION

In this paper we study the development of the electromagnetic cascade in the rotating electromagnetic field. First we derive the kinetic equations for the electrons, the positrons and the photons in the cascade. Second, we present the dimensional analysis and scaling for the kinetic cascade equations. In the limit when the growth rate is quite large $\Gamma \gg 1$ the angle between the momenta of the cascade particles and the electric field vector is small. This allows us to find how the cascade parameters such as the average particle momentum and the cascade growth rate depend on the frequency of the field rotation. It is shown that lower frequencies is preferable in the experiments devoting to the cascades observation. At the same time, the limitation of the attainable intensity due to prolific pair production is less strict for higher frequencies. Then, under the assumption that the most of particles have $\chi \gg 1$ the dependence of the cascade parameters on the electric field strength is found. Besides, for the distribution function "tails" corresponding to the particles with high values of quantum parameter $\chi \gg 1$ and with Lorentz factor $\gamma \gg \langle \gamma \rangle$, the analytical solution is found. The obtained formulae for the distribution functions and for the energy spectra agree fairly good with the results of the numerical simulations. Furthermore, the fit for the growth rate based on the results of the numerical simulations in a wide range of the parameters is proposed.

The electromagnetic cascades can arise in various realistic field configurations, particularly, in the field of circularly or linearly polarized standing wave [28]. In the field of the circularly polarized standing wave the cascade develops mostly in the B -node, where $B \approx 0$. Near this plane the field configuration is very close to the homogeneous rotating electric field. Certainly, some particles can leave the plane $B = 0$. However, we assume that this fact does not affect cascade dynamics much and the proposed theory fits well for the description of the electromagnetic cascades in the circularly polarized standing wave. The estimations also demonstrate that the cascade can arise in the crossed time-dependent electric and magnetic fields if the magnitude of the electric field is greater

than the magnitude of the magnetic field. In this case particle momenta are also concentrated along the distinguished direction and some simplifications of the kinetic equations are also possible. Thus, the proposed model for the electromagnetic cascades in rotating electric field can be used for analysis of the cascade dynamics in some other field configurations.

It follows from the numerical simulations that in the considered region of the parameters the big portion of the particles has $\chi \sim 1$ and can strongly affect the cascade development and the cascade growth rate. As far as the obtained distribution functions for the particles with $\chi \gg 1$ depend on the cascade growth rate, the proposed description of the "tails" of the distribution functions is not completely self-consistent. The contribution of the particles with $\chi \sim 1$ in Γ is especially substantial for the near-threshold cascades. Thus, the investigation of the distribution function component with $\chi \sim 1$ is important for experimental observation electromagnetic cascades in laser field at the lowest possible intensity level.

However, it is important to note that the predictions

of the proposed theory for the dependence of the cascade parameters on the frequency of the field rotation and for the distribution functions and the energy spectra of the high-energy cascade particles are in fairly good agreement with the results of the numerical simulations. The proposed model may be useful for the development of e^+e^- plasma sources and for the better understanding of some astrophysical processes. Furthermore, the obtained expressions might be also used to estimate the cascade parameters in the experiments by measuring the particle energy spectra.

Acknowledgments

We are grateful to A. M. Fedotov and N. B. Narozhny for fruitful discussions. This work has been supported by federal target program "The scientific and scientific-pedagogical personnel of innovation in Russia" and by the Russian Foundation for Basic Research.

-
- [1] G. A. Mourou *et al.*, Rev. Mod. Phys **78**, 309 (2006).
 - [2] M. Marklund and P. K. Shukla, Rev. Mod. Phys. **78**, 591 (2006).
 - [3] V. Yanovsky *et al.*, Opt. Express **16**, 2109 (2008).
 - [4] <http://www.extreme-light-infrastructure.eu>
 - [5] <http://www.hiper-laser.org>
 - [6] B. King, A. Di Piazza, C. H. Keitel, Phys. Rev. A **82**, 032114 (2010).
 - [7] S. S. Bulanov, V. D. Mur, N. B. Narozhny, J. Nees, V. S. Popov, Phys. Rev. Lett. **104**, 220404 (2010).
 - [8] A. Di Piazza, A. I. Milstein, C. Müller, Phys. Rev. A **82**, 062110 (2010).
 - [9] D. Burke *et al.*, Phys. Rev. Lett., **79**, 1626 (1997)
 - [10] C. Bamber *et al.*, Phys. Rev. D **60**, 092004 (1999).
 - [11] V. N. Baier, V. M. Katkov, and V. M. Strakhovenko, *Electromagnetic Processes at High Energies in Oriented Single Crystals* (Singapore, World Scientific, 1998).
 - [12] U. I. Uggerhoj, Rev. Mod. Phys. **77**, 1131-1171 (2005).
 - [13] I. V. Sokolov, N. M. Naumova, J. A. Nees, G. A. Mourou, Phys. Rev. Lett. **105**, 195005 (2010).
 - [14] H. Hu, C. Müller, C. H. Keitel, Phys. Rev. Lett. **105**, 080401 (2010).
 - [15] A. Ilderton, Phys. Rev. Lett. **106**, 020404 (2011).
 - [16] A. R. Bell and J. G. Kirk, Phys. Rev. Lett. **101**, 200403 (2008).
 - [17] A. M. Fedotov, N. B. Narozhny, G. Mourou, G. Korn, Phys. Rev. Lett. **105**, 080402 (2010).
 - [18] G. Breit and J. A. Wheeler, Phys. Rev. **46**, 1087 (1934).
 - [19] H. A. Bethe and W. Heitler, Proc. Roy. Soc. London A **146**, 83 (1934).
 - [20] F. Sauter, Z. Phys. **69**, 742 (1931).
 - [21] W. Heisenberg and H. Euler, Z. Phys. **98**, 714 (1936).
 - [22] J. Schwinger, Physical Review **82**, 664 (1951)
 - [23] E. Brezin and C. Itzykson, Phys. Rev. D **2**, 1191 (1970).
 - [24] H. K. Avetissian, A. K. Avetissian, G. F. Mkrtchian, and Kh. V. Sedrakian, Phys. Rev. E **66**, 016502 (2002).
 - [25] N. B. Narozhny, S. S. Bulanov, V. D. Mur, and V. S. Popov, Physics Letters A **330**, 1 (2004).
 - [26] N. B. Narozhny, S. S. Bulanov, V. D. Mur, and V. S. Popov, Zh. Eksp. Teor. Fiz. **129**, 14 (2006) [JETP **102**, 9 (2006)].
 - [27] S. X. Hu and A. F. Starace, Phys. Rev. Lett. **88**, 245003 (2002).
 - [28] E. N. Nerush *et al.*, Phys. Rev. Lett. **106**, 035001 (2011).
 - [29] V. B. Berestetskii, E. M. Lifshits, and L. P. Pitaevskii, *Quantum Electrodynamics* (Pergamon Press, New York, 1982).
 - [30] V. I. Ritus, Journal of Soviet Laser Research **6**. No.5, Sept.-Oct., 497 (1985); A. I. Nikishov, Journal of Soviet Laser Research **6**. No.6, Nov.-Dec., 619 (1985).
 - [31] E. Nerush, I. Kostyukov, arXiv:1101.4385v1 [physics.plasm-ph]
 - [32] G. R. Mocken, M. Ruf, C. Muller, and C. H. Keitel, Phys. Rev. A **81**, 022122 (2010).
 - [33] S. Agostinelli, *et al.*, Nuclear Instruments and Methods in Physics Research A **506**, 250 (2003).
 - [34] V. Anguelov and H. Vankov, J. Phys. G: Nucl. Part. Phys. **25**, 1755 (1999).
 - [35] I. V. Sokolov *et al.*, arXiv:1102.3685v1 [physics.plasm-ph]
 - [36] A. N. Timokhin, Mon. Not. R. Astron. Soc. **408**, 2092 (2010).
 - [37] N. V. Elkina *et al.*, Phys. Rev. ST Accel. Beams **14**, 054401 (2011).
 - [38] L. Landau, G. Rumer, Proc. Roy. Soc. **A166**, 213 (1938).
 - [39] B. Rossi, *High-Energy Particles* (Prentice-Hall, New York, 1952).
 - [40] M. Kh. Khokonov, J. Exp. Theor. Phys. **99**, 690 (2004).
 - [41] A. I. Akhiezer, N. P. Merenkov and A. P. Rekalov, J. Phys. G: Nucl. Part. Phys. **20**, 1499 (1994).
 - [42] E. Poisson, arXiv:gr-qc/9912045v1.
 - [43] M. Abramovitz, I. A. Stegun, *Handbook of Mathematical Functions with Formulas, Graphs, and Mathematical*

Tables (Dover Publications, New York, 1972).